

1 **A STUDY OF PHOTOSYNTHETIC BIOGAS UPGRADING BASED ON A HIGH**
2 **RATE ALGAL POND UNDER ALKALINE CONDITIONS**

3

4 Mariana Franco-Morgado¹, Cynthia Alcántara², Adalberto Noyola¹, Raúl Muñoz²,
5 Armando González Sánchez^{1*}

6 1. Instituto de Ingeniería, Universidad Nacional Autónoma de México, Circuito Escolar,
7 Ciudad Universitaria, 04510 Mexico City, Mexico

8 2. Department of Chemical Engineering and Environmental Technology, University of
9 Valladolid, C/Dr. Mergelina s/n, 47011 Valladolid, Spain

10 *Corresponding author: agonzalezs@iingen.unam.mx

11

12 **ABSTRACT**

13 Microalgal-bacterial processes have emerged as environmental friendly systems for the
14 cost-effective treatment of anaerobic effluents such as biogas and nutrients-laden
15 digestates. Environmental parameters such as temperature, irradiation, nutrient
16 concentration and pH effect the performance of the systems. In this paper, the potential of a
17 microalgal-bacterial photobioreactor operated under high pH (≈ 9.5) and high alkalinity to
18 convert biogas into biomethane was evaluated. The influence of the illumination regime
19 (continuous light supply vs 12 h/12 h light/dark cycles) on the synthetic biogas upgrading
20 efficiency, biomass productivity and nutrient removal efficiency was assessed in a High-
21 Rate Algal Pond interconnected to a biogas absorption bubble column. No significant
22 differences in the removal efficiency of CO₂ and H₂S ($91.5 \pm 2\%$ and $99.5\% \pm 0.5$,
23 respectively) were recorded regardless of the illumination regime. The high fluctuations of
24 the dissolved oxygen concentration during operation under light/dark cycles allowed to
25 evaluate the specific growth rate and the specific partial degradation rate of the microalgae
26 biomass by photosynthesis and respiration, respectively. The respiration reduced the net
27 microalgae biomass productivity under light/dark cycles compared with process operation
28 under the continuous light supply.

29 **Keywords:** alkaliphilic algal-bacterial consortium, biogas desulfurization, illumination
30 regime

31 INTRODUCTION

32 Biogas and digestate are the main byproducts from anaerobic digestion of organic waste.
33 The composition of raw biogas varies depending on the type of residue and conditions of
34 anaerobic digestion. A typical raw biogas composition accounts for CH₄ 40-70% vol, CO₂
35 15-60% vol, H₂S 0.005-2% vol, and trace contaminants like water, siloxanes and volatile
36 organic compounds (Muñoz et al., 2015) . Raw biogas can be used directly to generate heat
37 and/or power or injected into natural gas grids when its quality is comparable with that of
38 natural gas. The high content of CO₂ in raw biogas reduces its specific heating value and
39 increases its transportation costs. Another undesirable biogas component is H₂S, which is a
40 highly corrosive, toxic and malodorous gas (Noyola et al., 2006; Redondo et al., 2008). On
41 the other hand, anaerobic digestates are characterized by a high concentration of nutrients,
42 such as nitrogen (950 mg N-NH₄ L⁻¹) and phosphorus (415 mg P-PO₄³⁻ L⁻¹) which are
43 representative values from anaerobic sludge digestion made in municipal wastewater
44 treatment plants (Uggetti et al., 2014). These aqueous effluents must be treated to avoid
45 eutrophication of inland waterbodies and coastal areas (Batten et al., 2013). In this context,
46 there is crucial need to develop cost-effective and environmentally friendly technologies for
47 biogas upgrading and nutrient removal, based on both the versatile potential of biogas as a
48 renewable energy source and the high eutrophication impact of digestates.

49 Algal-bacterial processes have emerged as the only technology capable of simultaneously
50 upgrading biogas while recovering nutrients from digestates (Muñoz and Guieysse, 2006) .
51 On one hand, microalgae can photosynthetically use the CO₂ present in the biogas as a
52 carbon source while supporting the bacterial oxidation of H₂S via an in-situ O₂ supply
53 (González-Sánchez et al., 2008; de Godos et al., 2009; Bahr et al., 2014; Posadas et al.,
54 2013; Hernández et al., 2013) On the other, the use of digestate as a nutrient source for

55 microalgae and bacteria growth represents an opportunity to mitigate its eutrophication
56 potential (Batten et al., 2013; Franchino et al., 2013; Uggetti et al., 2014). Despite the
57 promising results obtained so far using algal-bacterial photobioreactors, biogas
58 bioconversion to biomethane is still limited by the low CO₂ mass transfer rates of this
59 technology (Yan et al., 2016). For instance, CO₂ removals ranging from 55 to 62 % were
60 recorded by Alcántara et al., (2015) and Lebrero et al., (2016) using High Rate Algal Pond
61 (HRAP) or bubble column algal-bacterial photobioreactors, which hindered the direct
62 injection of the upgraded biogas into natural gas grids.

63 In this context, pH has been identified as a critical parameter determining the mass transfer
64 rate of acidic gases such as H₂S and CO₂ in conventional gas-liquid contactors (Bahr et al.,
65 2014; González-Sánchez et al., 2008). Process operation at pH>9 mediate an enhancement
66 in the absorption rates of these biogas contaminants induced by chemical reactions
67 (González-Sánchez and Revah, 2007; Markou et al., 2014). The use of carbonated alkaline
68 cultivation media in algal-bacterial photobioreactors could support a long term efficient
69 biogas upgrading. In these systems, medium acidification induced by CO₂ and H₂S
70 absorption is counterbalanced by microalgae CO₂ uptake in the presence of light and CO₂
71 stripping under dark conditions. In addition, the use of extreme pH values promotes the
72 stability of microalgae populations by preventing contamination with predators or other
73 photosynthetic microorganisms (Lee, 2001). Despite the above mentioned advantages, the
74 understanding of biogas upgrading using alkaliphilic algal-bacterial consortia is very
75 limited.

76 This work aimed at evaluating the performance of a novel alkaliphilic microalgae-based
77 process deployed for synthetic biogas upgrading and nutrient removal under different

78 illumination regimes, assessing both the fate of carbon, nitrogen, phosphorous and sulphur
79 and biomass productivity through mass balances under steady state.

80

81 **MATERIAL AND METHODS**

82 **Microorganisms and culture conditions**

83 An alkali-tolerant microalgae culture (AMC) was used as a model photosynthetic
84 consortium throughout the entire experiment. The AMC was enriched from Texcoco soda
85 lake in Mexico City according to De los Cobos-Vasconcelos et al. (2015). A culture of
86 alkaliphilic sulphur oxidizing bacteria (ASB) was used as a model H₂S degrading
87 consortium (González-Sánchez and Revah, 2007). The mixed AMC/ASB culture was
88 grown in a mineral salt medium (MSM) composed of (g/L): Na₂CO₃ (4.03); NaHCO₃
89 (13.61); NaCl (1); K₂HPO₄ (1); K₂SO₄ (1); CaCl₂·H₂O (0.04); KNO₃ (2.52); MgCl₂·6H₂O
90 (0.2) and 2 mL of a micronutrient solution (Sorokin et al., 2001). The final pH of the MSM
91 medium was 9.3.

92

93 **Experimental set-up**

94 The experimental system consisted of a 25 L HRAP interconnected with a 0.35 L
95 Absorption Bubble Column (ABC) (Figure 1). The HRAP dimensions were 1.25 m long ×
96 0.25 m width × 0.14 cm deep, which entailed an effective illuminated area of 0.28 m². The
97 HRAP was illuminated at a photosynthetically active radiation (PAR) of 500 μmolm⁻²s⁻¹
98 (model LI250A, LI-COR, USA) provided by LED white-cool light lamps (model 511919,
99 Ecosmart, USA). The cultivation broth in the HRAP was continuously mixed using a six
100 bladed paddle wheel inducing a laminar flow regime at 15 cm s⁻¹. The ABC (0.80 m height

101 × 0.019 m of internal diameter) was interconnected to the HRAP via culture broth
102 recirculation.

103

Here Figure 1

104

105 **Operational conditions**

106 The HRAP was initially filled with 21 L of MSM and inoculated with four liters of AMC
107 containing a biomass concentration of 0.12 g TSS L⁻¹. The system was operated as fed-
108 batch under continuous illumination for 39 days. Four liters of algal cultivation broth were
109 drawn by day 20 and replaced with fresh ASB (0.2 g TSS L⁻¹) grown in MSM containing
110 10 g L⁻¹ of sodium thiosulfate (Na₂S₂O₃) as energy source. The mixed culture was then
111 cultivated in batch mode for 19 days (stage I). From day 40 to 166 (stage II), the HRAP
112 was continuously fed at a hydraulic retention time of 9.5 days with a 1.8 times diluted
113 MSM, mimicking the composition of a digestate, supplemented with 0.35 g Na₂S₂O₃ L⁻¹.
114 From day 167 to 269 (stage III), a gas mixture composed of CO₂ (30% vol), H₂S (0.5% vol)
115 and balanced with N₂ was considered as synthetic biogas, it was continuously bubbled at 22
116 L d⁻¹ through a porous stone located at the bottom of the ABC. The column was operated
117 co-currently at a liquid to synthetic biogas volumetric ratio (L/G) of 5 using the algal-
118 bacterial cultivation broth from the HRAP as scrubbing solution. From day 270 to 399
119 (stage IV), the illumination regime was set at a 12h:12 h light/dark photoperiod. The last
120 period (stage V) was operated for 117 days under similar operational conditions than those
121 imposed in stage II. Water evaporation rates were quantified and compensated by addition
122 of distilled water before sampling of the HRAP-ABC system.

123

Here table 1

124

125 Aliquots of 70 mL of HRAP cultivation broth and influent mineral salt medium were drawn
126 three times per week in order to monitor the concentration of TSS, total organic carbon
127 (TOC), inorganic carbon (IC), total nitrogen (TN), nitrite (NO_2^-), nitrate (NO_3^-), sulphate
128 (SO_4^{2-}), tiosulphate ($\text{S}_2\text{O}_3^{2-}$) and phosphate (PO_4^{3-}). The pH and dissolved oxygen (DO)
129 concentration of the cultivation broth were on-line recorded every 3 min. The composition
130 of synthetic biogas at the inlet and outlet of the ABC was daily monitored by non-
131 dispersive infrared sensor analysis. Finally, the elemental composition of the algal-bacterial
132 biomass was determined in stage III and IV.

133

134 **Analytical Procedures**

135 The concentration of TSS was measured according to Standard Methods (APHA, 2012).
136 Liquid samples were filtered through 0.45 μm Whatman filters prior determination of IC,
137 TOC, TN, PO_4^{3-} , SO_4^{2-} and $\text{S}_2\text{O}_3^{2-}$ concentrations. The concentration of IC, TOC and TN
138 was determined by a TOC-L CSH analyzer coupled to a TNM-L chemiluminescence
139 module (Shimadzu, Japan). The concentration of N-NO_3^- and N-NO_2^- were measured
140 spectrophotometrically with commercial Nitraver and Nitriver kits, respectively (HACH,
141 USA). $\text{S-S}_2\text{O}_3^{2-}$ concentration was measured by titration according to (Rodier J, 1988). The
142 concentration of S-SO_4^{2-} was analyzed according to the Standard Methods (WEF, 2012). P-
143 PO_4^{3-} concentration was analyzed using a Dionex ICS 2000 Ion Chromatograph (USA)
144 equipped with a IonPacAS23 column (250 \times 4 mm) eluted at 1 mL min^{-1} with a mobile
145 phase containing CO_3^{2-} and HCO_3^- at 4.5 y 0.8 mM, respectively. The elemental biomass
146 composition (C, N and S content) was determined from the biomass contained in aliquots

147 of 50 mL of cultivation broth centrifuged at 10,000 rpm (Avanti 123, Beckman Coulter,
 148 USA) and washed 3 times with Milli-Q water. The salt-free pellets were dried at 105°C for
 149 24h and grinded prior analysis in a Flash 2000 Elemental Analyzer CHNS-O Analyzer
 150 (Thermo Scientific, USA). The gas concentration of CO₂, O₂ and H₂S at the inlet and outlet
 151 of the ABC were analyzed with continuous nondispersive infrared sensor gas analyzer
 152 (Ultramat 23, Siemens, Germany). The dissolved oxygen concentration and pH were online
 153 determined using Applisens Z10023525 (Applikon, The Netherlands), Orion 9107BNMD
 154 (Thermo Scientific, USA) and temperature probes.

155

156 **Calculations**

157 A series of elemental mass balances under steady state, showed in equations 1, 2, 3 and 4
 158 and expressed as loading rates (Q_i = mass flow rate of component i /total liquid volume),
 159 allowed to assess the fate of carbon, nitrogen, phosphorus and sulphur under steady state in
 160 the HRAP-ABC.

$$161 \quad Q_{C_{Gin}} + Q_{C_{Lin}} = Q_{C_{Gout}} + Q_{C_{Lout}} + Q_{C_{-Xout}} + Q_{C_{stripping}} \quad (1)$$

$$162 \quad Q_{N_{Lin}} = Q_{N_{Lout}} + Q_{N_{-Xout}} \quad (2)$$

$$163 \quad Q_{P_{Lin}} = Q_{P_{Lout}} + Q_{P_{-Xout}} \quad (3)$$

$$164 \quad Q_{S_{Gin}} + Q_{S_{Lin}} = Q_{S_{Gout}} + Q_{S_{Lout}} + Q_{S_{-Xout}} \quad (4)$$

165

166 Where $Q_{i, in}$ and $Q_{i, out}$ represent the inlet and outlet mass loading rates, respectively, of all
 167 species (i = carbon-C, nitrogen-N, phosphorous-P and sulphur-S) in liquid (L) and gas (G)
 168 phases. Q_{i-X} represents the loading rate of each i contained in the biomass present in the
 169 effluent. $Q_{c, stripping}$ represents the C as CO₂ lost by stripping from the HRAP. The CO₂

170 stripping from the HRAP was evaluated from equation 5 including the discrete IC
 171 measurements together with the corresponding pH. The dissolved CO₂ (DCO₂) was
 172 calculated as a function of pH, according to equation 6.

$$173 \text{ CO}_2 \text{ stripping rate} = \frac{V_H}{V_T} k_L a_H \left(\frac{CO_{2air}}{H_{CO_2}} - DCO_2 \right) \quad (5)$$

$$174 [DCO_2] = \frac{IC}{1 + \frac{K_1}{[H^+]} + \frac{K_1 * K_2}{[H^+]^2}} \quad (6)$$

175 Where V_H and V_T represent the volume of the aqueous phase in the HRAP and total
 176 aqueous volume in the HRAP+ABC. H_{CO₂} represents the CO₂ Henry constant (1.1
 177 dimensionless at 20 °C). K_La_H represents the global volumetric gas-liquid mass transfer
 178 coefficient (20 d⁻¹) in the HRAP, which was experimentally determined . CO_{2air} is the
 179 carbon dioxide concentration in air (350 ppm_v = 1.1×10⁻⁵ mol L⁻¹). K₁ and K₂ are the
 180 dissociation constants for the system CO₂-H₂O (4.66×10⁻⁷ mol L⁻¹ and 4.67×10⁻¹¹ mol L⁻¹,
 181 respectively) and [H⁺] is the proton concentration in the cultivation broth (mol L⁻¹).

182

183 **Assessment of the specific growth and partial degradation rates of microalgae under**
 184 **light/dark cycles**

185 The fluctuations of the DO measurements recorded during stage IV under steady state were
 186 described using a dynamic oxygen mass-balance applied to the liquid phase (Eq. 7). This
 187 mass balance was used to estimate either the volumetric oxygen production or consumption
 188 (rO₂) associated to microalgae biomass metabolism, accounting for the variation on the
 189 temperature.

$$190 \frac{dDO}{dt} = \frac{F}{V_T} (DO_{in} - DO) + \frac{V_C}{V_T} k_L a_C \left(\frac{O_{2g}}{H_{O_2}} - DO \right) + \frac{V_H}{V_T} k_L a_H \left(\frac{O_{2air}}{H_{O_2}} - DO \right) +$$

$$191 \frac{V_H}{V_T} r_{O_2} - R_{O_2-S} \quad (7)$$

192 Where V_C represents the volume of the aqueous phase in the ABC (0.3 L), r_{O_2} represents
 193 the microalgal oxygen consumption or production rate ($\text{mol L}^{-1} \text{d}^{-1}$), H_{O_2} represents the
 194 oxygen Henry constant (32 dimensionless at 20 °C). $K_L a_C$ stands the global volumetric gas-
 195 liquid mass transfer coefficient (141d^{-1}) in the ABC, which was experimentally determined
 196 using the gassing-out method. R_{O_2-S} was estimated to $0.0007 \text{mol O}_2 \text{L}^{-1} \text{d}^{-1}$ based on the
 197 sulphur mass balance under steady state conditions, assuming complete oxidation to
 198 sulphate.

199 The evaluation of the specific growth rate (μ_{light}) and the specific partial degradation rate
 200 (μ_{dark}) of the microalgae biomass by photosynthesis and by respiration, respectively, was
 201 based on the assumption of a 15 % w/w biomass loss by respiration during the 12 h dark
 202 period (Grobbelaar and Soeder, 1985). This entails a $\mu_{\text{light}}/\mu_{\text{dark}}$ ratio of -4.2. μ_{light} can be
 203 expressed in terms of the photosynthetic oxygen/biomass ($y_{O_2/X}^p$) yield (de los Cobos-
 204 Vasconcelos et al., 2015) and the oxygen production rate ($r_{O_2}^p$). Similarly, μ_{dark} can be
 205 defined in terms of an endogenous respiration oxygen/biomass ($y_{O_2/X}^r$) yield and its
 206 corresponding oxygen respiration rate ($r_{O_2}^r$). Therefore, the overall $y_{O_2/X}^r$ was evaluated
 207 according to equation (8) for several light/dark cycles exposed to constant temperature
 208 fluctuations. $r_{O_2}^p$ and $r_{O_2}^r$ represent averaged values for a set of continuous days reaching
 209 uniform temperature fluctuations.

$$210 \quad y_{O_2/X}^r = 4.2 \frac{(r_{O_2}^r)(y_{O_2/X}^p)}{r_{O_2}^p} \quad (8)$$

211 The net volumetric biomass productivity (P_x) was evaluated from the condition of steady
 212 state for a continuous cultivation (see equation 9).

$$213 \quad P_x = D \cdot X = (\mu_{\text{light}} - \mu_{\text{dark}}) \cdot X = \frac{r_{O_2}^p}{y_{O_2/X}^p} - \frac{r_{O_2}^r}{y_{O_2/X}^r} \quad (9)$$

214 Where D is the dilution rate (d^{-1}) and X the experimental biomass concentration (g TSS L⁻¹).
215
216

217

218

219

220

RESULTS AND DISCUSSION

Synthetic biogas upgrading performance

221 The removal efficiencies of CO₂ and H₂S during stage III accounted for $89 \pm 4\%$ and 99.5
222 $\pm 0.5\%$, respectively, and $94 \pm 1\%$ and $99.5 \pm 0.5\%$, respectively, during stage IV. The
223 similar pH values recorded during both stages explain the comparable synthetic biogas
224 upgrading performance regardless of the illumination regime. Thus, in spite of the
225 continuous feeding of CO₂ and H₂S during stage III the pH remained constant at ≈ 9.5 likely
226 due to high buffer capacity (alkalinity) of cultivation medium and the high photosynthetic
227 activity of the AMC under continuous illumination. However, pH fluctuated from 9.3 to 9.7
228 during stage IV as a result of the periodic medium acidification during the dark period due
229 to CO₂ and H₂S absorption, and the microalgae-based regeneration of alkalinity during the
230 light period. In this context, the increase in pH mediated by microalgae growth during the
231 illuminated period is expected to support a high biogas upgrading performance during
232 outdoors operation. These high CO₂ and H₂S removal efficiencies were also supported by
233 the high L/G ratio of 5), which prevented a deterioration in the CO₂ /H₂S mass transfer
234 induced by a decrease in the pH of the cultivation medium in the ABC (Serejo et al. 2015).
235 However, high L/G ratios often promote a high O₂ stripping from the recirculation medium
236 to the biomethane, with the concomitant contamination of the upgraded biogas. In this
237

238 study, the oxygen concentration in upgraded synthetic biogas averaged 2.6% v/v during
239 stage III and IV. According to the Mexican regulation (NOM-001-SECRE 2010) oxygen
240 concentration in biomethane must be lower than 0.20% v/v. This requires an optimization
241 of the L/G ratio or the implementation of operational strategies devoted to decrease the
242 oxygen liquid concentration prior recirculation to the ABC (Toledo-Cervantes et al., 2016).
243 The complete removal of H₂S recorded in stage III and IV promoted the accumulation of
244 SO₄²⁻ in the cultivation broth concomitantly with synthetic biogas upgrading. The high DO
245 concentration prevailing in the HRAP during the entire experimental period (even during
246 dark periods DO remained > 2 mg O₂ L⁻¹) supported a complete oxidation of H₂S to
247 sulphate (González-Sánchez and Revah, 2007) (Table 2). The concentration of S-SO₄²⁻
248 achieved during steady state in stages III and IV were 0.32 ± 0.02 g L⁻¹ and 0.34 ± 0.05 g L⁻¹,
249 respectively.

250

251 **Photobioreactor performance**

252 The batch cultivation during stage I supported an increase in biomass concentration in the
253 HRAP-ABC system from 0.12 g TSS L⁻¹ to 0.77 g TSS L⁻¹ by day 39, concomitant with a
254 decrease in IC concentration from 1.25 g C L⁻¹ to 0.21 g C L⁻¹ (Figure 2). Process operation
255 under continuous illumination at a HRT of 9.5 days entailed steady state biomass
256 concentration of 0.72 ± 0.04 g TSS L⁻¹ during stage II. The continuous supply of MSM
257 mediated an increase of the IC concentration in the HRAP, which stabilized at 1.13 ± 0.09
258 g C L⁻¹ from day 120 till 166. Synthetic biogas supply during stage III under continuous
259 illumination resulted in an increase in biomass concentration up to 1.23 ± 0.05 g TSS L⁻¹,
260 which suggested that microalgae growth was limited by CO₂ concentration during stage II
261 at the high pH value prevailing in the cultivation broth (pH=10.03 ± 0.16). The 50%

262 reduction in light energy supply mediated by process operation under 12h/12h light /dark
263 cycles induced a decrease in biomass concentration from 1.23 ± 0.05 g TSS L⁻¹ to steady
264 state values of 0.23 ± 0.05 g TSS L⁻¹ by the end of stage IV. This decrease in TSS
265 concentration entailed a reduction in the volumetric biomass productivity from 0.129 to
266 0.023 g TSS L⁻¹ d⁻¹, but did not impact on the concentration of IC in the HRAP, which
267 remained constant at 1.02 ± 0.06 g C L⁻¹ (Table 2 and Figure 2) probably due to the CO₂
268 stripping as it is explained below. A detailed explanation of the mechanisms underlying the
269 unexpectedly low biomass productivity is provided below. Process operation under
270 continuous illumination during stage V supported an increase in biomass concentration and
271 productivities up to steady state values of 0.94 ± 0.09 g TSS L⁻¹ and 0.098 g TSS L⁻¹ d⁻¹
272 (Table 2). The absence of synthetic biogas supply during stage V resulted in an increase in
273 the pH up to 10.23 ± 0.05 and in the expected decrease in IC concentration to steady state
274 values of 0.86 ± 0.12 g C L⁻¹ via biomass assimilation (Figure 2).

275

Here figure 2

276

277 The average removal efficiencies of nitrogen and phosphorous during stages III, IV and V
278 are shown in Table 2. Similar nutrient removal efficiencies were achieved during stage III
279 and V, while the decrease in biomass productivity recorded in stage IV resulted in a
280 significant decrease in the removal efficiency of phosphate. An experimental error in the
281 determination of nitrate concentrations might explain the unexpectedly high nitrate
282 removals recorded during stage IV (comparable to stage III and IV), since no noteworthy
283 differences were observed in the elemental composition of the biomass along the three last
284 operational stages and N-NO₂⁻ concentrations were very low (≈ 0.0004 mg N-NO₂⁻.L⁻¹). A

285 potential N₂O production in the system was also ruled out due to the relatively high DO
286 present in the HRAP during stage IV (> 2mg O₂ L⁻¹), which prevented nitrate
287 denitrification (Wang et al., 2008).

288

Here table 2

289

290

291 **C, N, P and S mass balances**

292 Mass balance calculations for the main elemental components were conducted in the
293 experimental system under steady state in stages III, IV and V.

294

Here figure 3

295

296 The carbon present in the synthetic biogas as CO₂ accounted for approx. 40 % of the
297 inorganic carbon inlet load in stage III and IV (Figure 3 a). Dissolved inorganic carbon
298 accounted for 58 % of the output carbon from the system. On the other, the carbon present
299 as biomass in the liquid effluent represented 30 % of the output carbon during continuous
300 illumination, while this share decreased to 7 % under light/dark cycles as a result of the
301 limited microalgal productivity. This limited microalgae growth during stage IV resulted in
302 an enhanced carbon stripping, which increased from 5 to 12 %. The restoration of
303 continuous illumination in the absence of synthetic biogas in stage V increased the share of
304 inorganic carbon assimilated into biomass, which accounted for 37 % of the total output
305 carbon, thereby minimizing carbon stripping. The nitrogen assimilated as biomass
306 accounted for 54, 14 and 50 % of the output nitrogen in stages III, IV and V, respectively

307 (Figure 3b). Similarly, the phosphorous fixed in the biomass represented 17, 3 and 14 % of
308 the output phosphorous in stages III, IV and V, respectively. For both nutrients, the share in
309 the output streams was correlated with biomass productivity since no difference in the
310 biomass N and P content was recorded. Finally, the H₂S present in the synthetic biogas
311 accounted for 12 and 10% of the inlet Sulphur in stages III and IV, respectively. This share
312 was significantly lower than the sulphur present as thiosulphate in the feed. Both reduced
313 forms of sulphur were completely oxidized to sulphate, which represented 99.5% of the
314 output sulphur in stage III, IV and V.

315

316 **Effect of light/dark cycles on the biomass productivity**

317 During the illuminated period in stage IV, microalgal photosynthesis was responsible of a
318 net oxygen production in the HRAP. However, in the dark period, the microalgae and
319 sulfide oxidizing bacteria consumed by respiration the dissolved oxygen present in the
320 cultivation broth, with a concomitant production of CO₂ (Bahr et al., 2014; Masojídek and
321 Koblížek, 2004). Hence, the dynamic balance between microalgae growth and endogenous
322 biomass consumption entailed a steady state biomass concentration 0.2 g TSS L⁻¹, which
323 were significantly lower than the expected value derived from a 50% reduction in light
324 supply. In the absence of light supply, the microalgae consumed their intracellular organic
325 carbon (i.e. carbohydrates) for cell maintenance, which was likely responsible of the lower
326 biomass concentrations recorded. Figure 4, based on the estimated volumetric oxygen
327 production and consumption (rO₂) rates from equation 7, shows that endogenous
328 respiration activity was similar to the photosynthetic activity responsible of microalgae
329 growth.

330

Here figure 4

331

332 Two different temperature fluctuation trends can be observed in Figure 4, since the HRAP-
333 ABC was exposed to the daily outdoors temperature fluctuations. These variations in the
334 temperature of the cultivation broth influenced the extent of the oxygen production and
335 endogenous respiration rates of the algal-bacterial consortium. From day 370 to 377, the
336 temperature fluctuated from 13 to 24°C, while for days 387 to 396 the range was 16 to
337 28°C. This difference of 4 °C in the temperature fluctuation range induced a 60 % increase
338 in both μ_{light} , μ_{dark} and biomass productivity (Table 3). Therefore, the microalgae
339 productivities estimated were highly affected by the lower temperatures, which correlated
340 with the decrease in the photosynthetic growth rates. The endogenous respiration yield,
341 $y_{O_2/X}^r$, was up to three times higher than the photosynthetic oxygen production yield,
342 $y_{O_2/X}^p$, and showed an inverse correlation with temperature. The $y_{O_2/X}^r$ here estimated were
343 in agreement with the respiration yields typically reported in microalgal cultures (0.0034-
344 0.124 mol O₂/gTSS) (Le Borgne and Pruvost, 2013; Ruiz-Martinez et al., 2016). The novel
345 methodology for the calculation of microalgae biomass productivity here developed based
346 on continuous DO measurements was validated by the empirical biomass productivity
347 estimated on the empirical measurements of the dilution rate and effluent biomass
348 concentration (Table 3).

349

Here table 3

350

351

352 **Conclusions**

353 Alkaliphic algal-bacterial consortia were shown as an effective platform to bioconvert
354 biogas into biomethane. Microalgal photosynthesis was able to effectively regenerate the
355 alkalinity consumed during CO₂ and H₂S absorption even during light/dark illumination
356 regimes similar to those prevailing under outdoors conditions. Carbon and nutrient recovery
357 was a function of the biomass productivity, which itself depended on the photobioreactor
358 illumination regime and temperature. The endogenous microalgae respiration during the
359 dark period was likely responsible of the higher decrease in biomass compared to that
360 expected from a 50% reduction in light supply.

361

362 **Acknowledgements**

363 This research was supported by the National Science Foundation of Mexico (CB-Conacyt
364 168288), Mexican Secretary of Marine (SEMAR-Conacyt 207151), Mexican Secretary of
365 Energy (SENER-Conacyt 247006) and by the internal project IIUNAM 4328. The
366 analytical assistance of Dr. Juan Gabriel Viguera Ramírez and the financial support of
367 projects CTM2015-70442-R (MINECO-FEDER) and VA024U14 are also gratefully
368 acknowledged. This research work was performed in the IIUNAM-Environmental
369 Laboratory with ISO9000 certificate.

370

371 **References**

- 372 Alcantara, C., Garcia-Encina, P.A., Muñoz, R., 2015. Evaluation of the simultaneous
373 biogas upgrading and treatment of centrates in a high-rate algal pond through C, N and
374 P mass balances. *Water Sci. Technol.* 72, 150–157. doi:10.2166/wst.2015.198
- 375 Bahr, M., Díaz, I., Dominguez, A., González Sánchez, A., Muñoz, R., 2014. Microalgal-

376 biotechnology as a platform for an integral biogas upgrading and nutrient removal
377 from anaerobic effluents. *Environ. Sci. Technol.* 48, 573–581. doi:10.1021/es403596m
378 Batten, D., Beer, T., Freischmidt, G., Grant, T., Liffman, K., Paterson, D., Priestley, T.,
379 Rye, L., Threlfall, G., 2013. Using wastewater and high-rate algal ponds for nutrient
380 removal and the production of bioenergy and biofuels. *Water Sci. Technol.* 67, 915–
381 24. doi:10.2166/wst.2012.618
382 De Godos, I., González, C., Becares, E., García-Encina, P. a, Muñoz, R., 2009.
383 Simultaneous nutrients and carbon removal during pretreated swine slurry degradation
384 in a tubular biofilm photobioreactor. *Appl. Microbiol. Biotechnol.* 82, 187–194.
385 doi:10.1007/s00253-008-1825-3
386 de los Cobos-Vasconcelos, D., García-Cruz, E.L., Franco-Morgado, M., González-Sánchez,
387 A., 2015. Short-term evaluation of the photosynthetic activity of an alkaliphilic
388 microalgae consortium in a novel tubular closed photobioreactor. *J. Appl. Phycol.*
389 doi:10.1007/s10811-015-0612-7
390 Franchino, M., Comino, E., Bona, F., Riggio, V. a, 2013. Growth of three microalgae
391 strains and nutrient removal from an agro-zootechnical digestate. *Chemosphere* 92,
392 738–44. doi:10.1016/j.chemosphere.2013.04.023
393 González-Sánchez, A., Revah, S., 2007. The effect of chemical oxidation on the biological
394 sulfide oxidation by an alkaliphilic sulfoxidizing bacterial consortium. *Enzyme*
395 *Microb. Technol.* 40, 292–298. doi:10.1016/j.enzmictec.2006.04.017
396 González-Sánchez, A., Revah, S., Deshusses, M.A., 2008. Alkaline Biofiltration of H₂S
397 Odors. *Environ. Sci. Technol.* 42, 7398–7404. doi:10.1021/es800437f
398 Grobbelaar, J.U., 2004. Algal Nutrition, in: Amos, R. (Ed.), *Handbook of Microalgal*
399 *culture:Biotechnology of Applied Phycology*. Blackwell Publishing, UK, pp. 95--115.

400 Grobbelaar, J.U., Soeder, C.J., 1985. Respiration losses in planktonic green algae cultivated
401 in raceway ponds. *J. Plankton Res.* 7, 497–506. doi:10.1093/plankt/7.4.497

402 Hernández, D., Riaño, B., Coca, M., García-González, M.C., 2013. Treatment of agro-
403 industrial wastewater using microalgae-bacteria consortium combined with anaerobic
404 digestion of the produced biomass. *Bioresour. Technol.* 135, 598–603.
405 doi:10.1016/j.biortech.2012.09.029

406 Le Borgne, F., Pruvost, J., 2013. Investigation and modeling of biomass decay rate in the
407 dark and its potential influence on net productivity of solar photobioreactors for
408 microalga *Chlamydomonas reinhardtii* and cyanobacterium *Arthrospira platensis*.
409 *Bioresour. Technol.* 138, 271–276. doi:10.1016/j.biortech.2013.03.056

410 Lebrero, R., Toledo-Cervantes, A., Muñoz, R., del Nery, V., Foresti, E., 2016. Biogas
411 upgrading from vinasse digesters: a comparison between an anoxic biotrickling filter
412 and an algal-bacterial photobioreactor. *J. Chem. Technol. Biotechnol.* 91, 2488–2495.
413 doi:10.1002/jctb.4843

414 Lee, Y., 2001. Microalgal mass culture systems and methods : Their limitation and
415 potential 307–315.

416 Markou, G., Vandamme, D., Muylaert, K., 2014. Microalgal and cyanobacterial cultivation:
417 The supply of nutrients. *Water Res.* 65, 186–202. doi:10.1016/j.watres.2014.07.025

418 Masojídek J, Koblížek M, T.G., 2004. Photosynthesis in Microalgae, in: Amos, R. (Ed.),
419 *Microalgal Culture: Biotechnology of Applied Phycology*. Blackwell Publishing, UK,
420 pp. 20–39.

421 Muñoz, R., Guieysse, B., 2006. Algal-bacterial processes for the treatment of hazardous
422 contaminants: a review. *Water Res.* 40, 2799–815. doi:10.1016/j.watres.2006.06.011

423 Muñoz, R., Meier, L., Diaz, I., Jeison, D., 2015. A review on the state-of-the-art of

424 physical/chemical and biological technologies for biogas upgrading. *Rev. Environ.*
425 *Sci. Biotechnol.* 14, 727–759. doi:10.1007/s11157-015-9379-1

426 NOM-001-SECRE-, 2010. Especificaciones del gas natural. *Diario Oficial. Secretaria de*
427 *Energia, Mexico.*

428 Noyola, A., Morgan-Sagastume, J.M., López-Hernández, J.E., 2006. Treatment of Biogas
429 Produced in Anaerobic Reactors for Domestic Wastewater: Odor Control and
430 Energy/Resource Recovery. *Rev. Environ. Sci. Bio/Technology* 5, 93–114.
431 doi:10.1007/s11157-005-2754-6

432 Posadas, E., Garcia-Encina, P.A., Soltau, A., Dominguez, A., Diaz, I., Muñoz, R., 2013.
433 Carbon and nutrient removal from centrates and domestic wastewater using algal-
434 bacterial biofilm bioreactors. *Bioresour. Technol.* 139, 50–58.
435 doi:10.1016/j.biortech.2013.04.008

436 Redondo, R., Machado, V.C., Baeza, M., Lafuente, J., Gabriel, D., 2008. On-line
437 monitoring of gas-phase bioreactors for biogas treatment: hydrogen sulfide and sulfide
438 analysis by automated flow systems. *Anal. Bioanal. Chem.* 391, 789–98.
439 doi:10.1007/s00216-008-1891-5

440 Rodier J, 1988. *Analisis de las aguas.* Omega S.A., Barcelona, Spain.

441 Ruiz-Martinez, A., Serralta, J., Seco, A., Ferrer, J., 2016. Behavior of mixed
442 Chlorophyceae cultures under prolonged dark exposure. Respiration rate modeling.
443 *Ecol. Eng.* 91, 265–269. doi:10.1016/j.ecoleng.2016.02.025

444 Serejo, M.L., Posadas, E., Boncz, M.A., Blanco, S., García-Encina, P., Muñoz, R., 2015.
445 Influence of biogas flow rate on biomass composition during the optimization of
446 biogas upgrading in microalgal-bacterial processes. *Environ. Sci. Technol.* 49, 3228–
447 3236. doi:10.1021/es5056116

448 Sorokin, D.Y., Lysenko, A.M., Mityushina, L.L., Tourova, T.P., Jones, B.E., Rainey, F.A.,
449 Robertson, L.A., Kuenen, G.J., 2001. nov . and Thioalkalimicrobium sibericum sp .
450 nov ., and Thioalkalivibrio versutus gen . nov ., sp . nov ., Thioalkalivibrio nitratis sp .
451 nov . and Thioalkalivibrio denitrificans sp . nov ., novel obligately alkaliphilic and
452 obligately chemolithoautotroph 565–580.

453 Toledo-Cervantes, A., Serejo, M.L., Blanco, S., Pérez, R., Lebrero, R., Muñoz, R., 2016.
454 Photosynthetic biogas upgrading to bio-methane: Boosting nutrient recovery via
455 biomass productivity control. Algal Res. 17, 46–52. doi:10.1016/j.algal.2016.04.017

456 Uggetti, E., Sialve, B., Latrille, E., Steyer, J.-P., 2014. Anaerobic digestate as substrate for
457 microalgae culture: the role of ammonium concentration on the microalgae
458 productivity. Bioresour. Technol. 152, 437–43. doi:10.1016/j.biortech.2013.11.036

459 Wang, J., Peng, Y., Wang, S., Gao, Y., 2008. Nitrogen Removal by Simultaneous
460 Nitrification and Denitrification via Nitrite in a Sequence Hybrid Biological Reactor.
461 Chinese J. Chem. Eng. 16, 778–784. doi:10.1016/S1004-9541(08)60155-X

462 WEF, A.A. and A.P.H.A., 2012. Water Environment Federation, Standard methods for the
463 examination of water and wastewater.

464 Yan, C., Muñoz, R., Zhu, L., Wang, Y., 2016. The effects of various LED (light emitting
465 diode) lighting strategies on simultaneous biogas upgrading and biogas slurry nutrient
466 reduction by using of microalgae Chlorella sp. Energy 106, 554–561.
467 doi:10.1016/j.energy.2016.03.033

468

469

470 **Legends of figures**

471

472 **Figure 1.** Experimental set-up used for the alkaliphilic synthetic biogas upgrading. Dashed
473 lines represent synthetic biogas streams and continuous lines represent liquid streams.

474

475 **Figure 2.** Time course of concentration of biomass (Δ) and inorganic carbon (\bullet) during the
476 operation of the HRAP-ABC.

477

478 **Figure 3.** Carbon (a), nitrogen (b), phosphorous (c) and sulphur (d) mass balances for
479 stages III, IV and V under steady state in the experimental HRAP-ABC. Numbers above
480 bars represent the respective input and output loading rates ($\text{g L}^{-1}\text{d}^{-1}$).

481

482 **Figure 4.** Time course of the estimated oxygen production and consumption rates (a) and
483 temperature (b) in the cultivation broth during the light and dark periods. Shade areas
484 represent dark periods.

Table 1[Click here to download Table: Table 1.docx](#)**Table 1.** Operational conditions deployed in the experimental system HRAP-ABC.

| Stage | Period (d) | MSM condition | Operation mode | Illumination | Synthetic biogas supply | |
|------------|------------|---------------|---------------------------|-------------------------|-------------------------|-------------|
| I | 0-39 | (a) | Fed-batch | 24 h | No | |
| II | 40-166 | (b) | Continuous HRT = 9.5 d | 24 h | No | |
| III | 167-269 | (b) | Continuous HRT = 9.5 d | 24 h | Yes | GRT= 23 min |
| IV | 270-399 | (b) | Continuous HRT = 9.5 d | 12 h/12 h light/dark | Yes | |
| V | 400-517 | (b) | Continuous HRT = 9.5 d | 24 h | No | |

(a) Cultivation in MSM

(b) Cultivation in 1.8 diluted MSM containing $0.35 \text{ g Na}_2\text{S}_2\text{O}_3 \text{ L}^{-1}$

GRT-Gas residence time; HRT-Hydraulic residence time

Table 2[Click here to download Table: Table 2.docx](#)**Table 2.** Summary of the environmental and operational parameters in the HRAP-ABC system under steady state during Stages III, IV and V.

| Parameter | Stage III | Stage IV | Stage V |
|--|---------------|---|---------------|
| <i>P_x</i> (g L ⁻¹ d ⁻¹) | 0.129 ± 0.005 | 0.023 ± 0.001 | 0.100 ± 0.012 |
| <i>X</i> (g TSS L ⁻¹) | 1.23 ± 0 | 0.23 ± 0.05 | 0.94 ± 0.05 |
| DO (mg L ⁻¹) | 10.8 ± 0.6 | Light/Dark 11.4 ± 0.5 / 2.8 ± 0.1 | 10.8 ± 1.3 |
| pH | 9.53 ± 0.05 | Light/Dark 9.71 ± 0.00 / 9.39 ± 0.00 | 10.23 ± 0.05 |
| T (°C) | 19.2 ± 2.6 | 22.8 ± 4.0 | 23.9 ± 1.7 |
| N-NO₃⁻ removal (%) | 52 ± 9 | 41 ± 5 | 55 ± 21 |
| P-PO₄³⁻ removal (%) | 24 ± 8 | 12 ± 7 | 29 ± 11 |
| C-biomass (%w) | 44.7 | 44.5 | 50.0 |
| N-biomass (%w) | 8.7 | 7.7 | 8.0 |
| S-biomass (%w) | 0.8 | 0.6 | 0.1 |
| P-biomass (%w)* | 1.0 | 1.0 | 1.0 |

* (Grobbelaar, 2004)

Table 3[Click here to download Table: Table 3.docx](#)

Table 3. Influence of photosynthesis and respiration on the kinetic parameters and biomass productivity during light/dark cycles, based on the assumption of a 15 % w/w biomass lost by respiration during a 12 h dark period.

| Temp. Range (°C) | Kinetic parameters | | | | | Biomass productivity (<i>P_x</i>) | |
|---|--|-------------|------------------------|----------------------|---------------------|---|-------------|
| | $r_{O_2}^p$ | $r_{O_2}^r$ | $y_{O_2/X}^r$ | μ_{light} | μ_{dark} | $\frac{r_{O_2}^p}{y_{O_2/X}^p} - \frac{r_{O_2}^r}{y_{O_2/X}^r}$ | $D \cdot X$ |
| | (mol L ⁻¹ d ⁻¹) | | (mol g ⁻¹) | d ⁻¹ | | g L ⁻¹ d ⁻¹ | |
| 13 to 24 | 0.0010 | 0.0009 | 0.2441 | 0.0786 | -0.0184 | 0.0120 | 0.0208 |
| 16 to 28 | 0.0016 | 0.0006 | 0.1017 | 0.1258 | -0.0295 | 0.0193 | 0.0208 |

Figure 1
[Click here to download high resolution image](#)

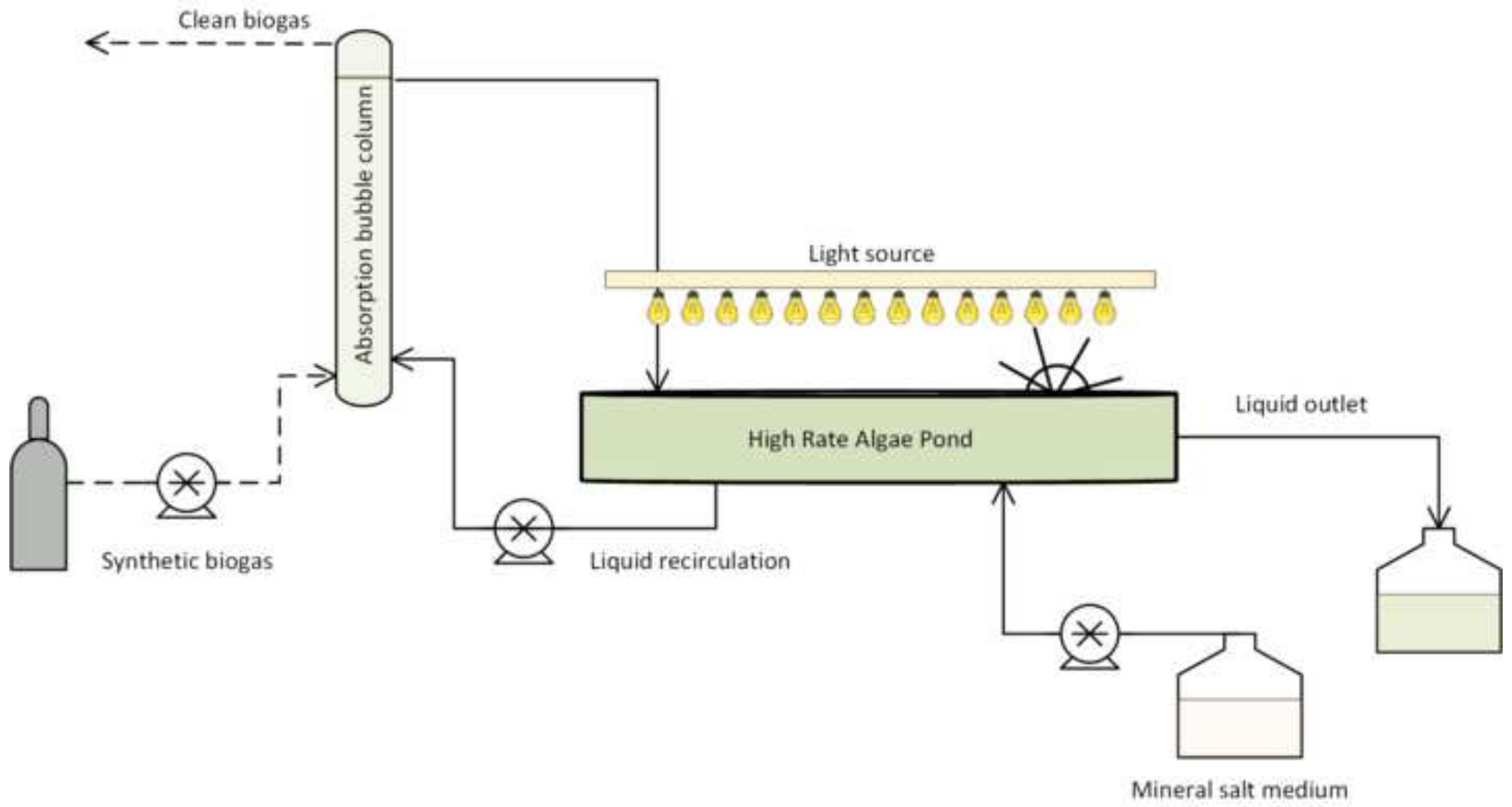


Figure 2
[Click here to download high resolution image](#)

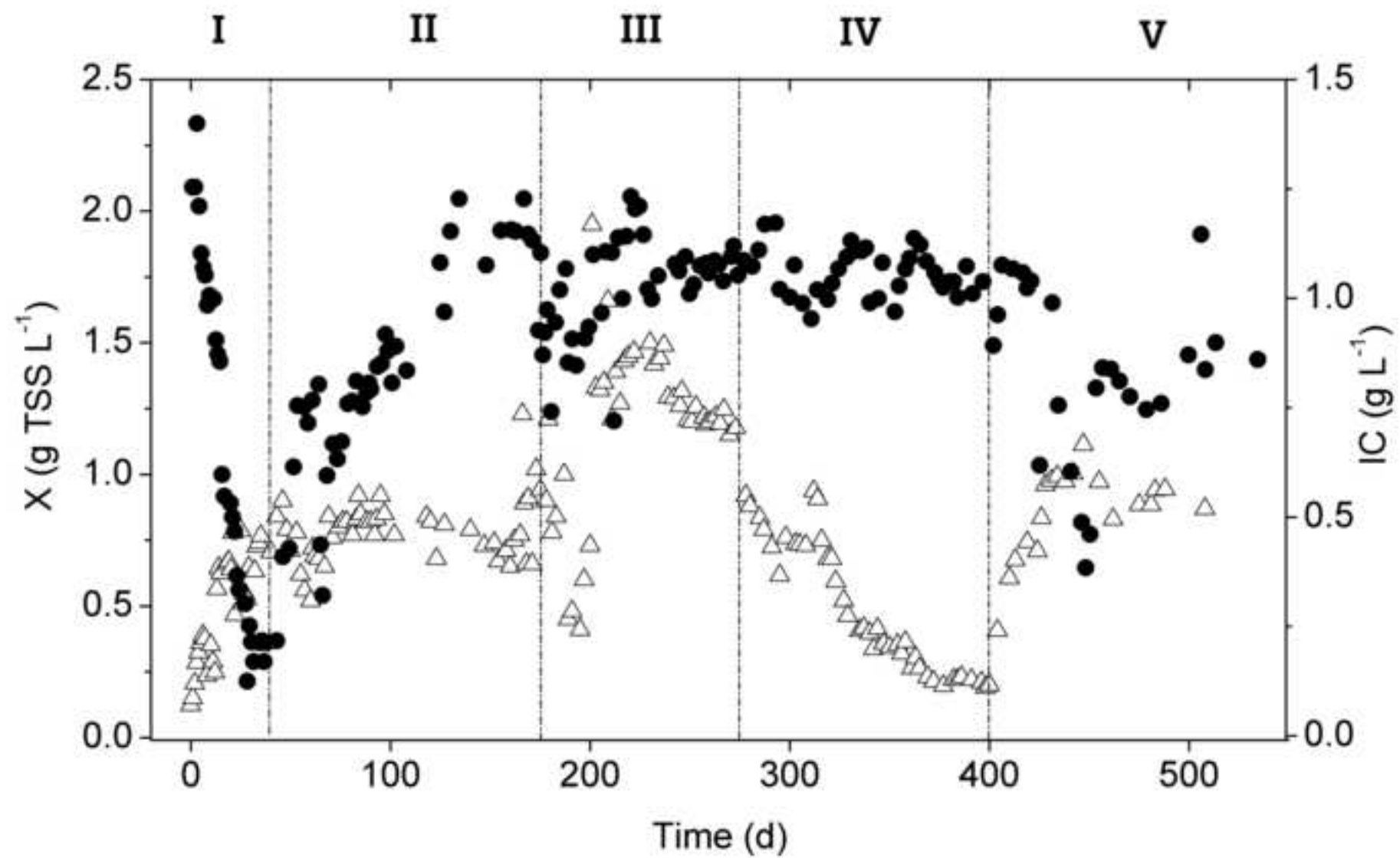


Figure 3
[Click here to download high resolution image](#)

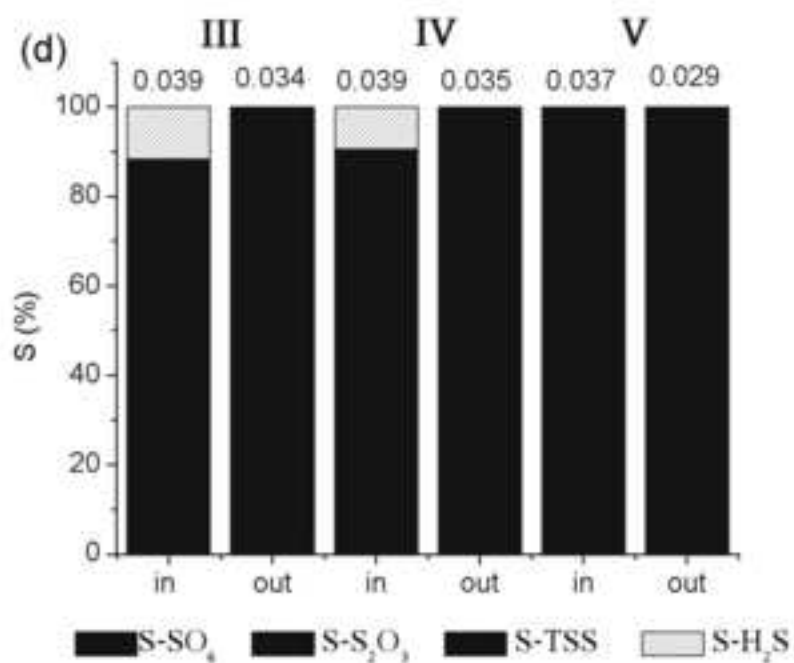
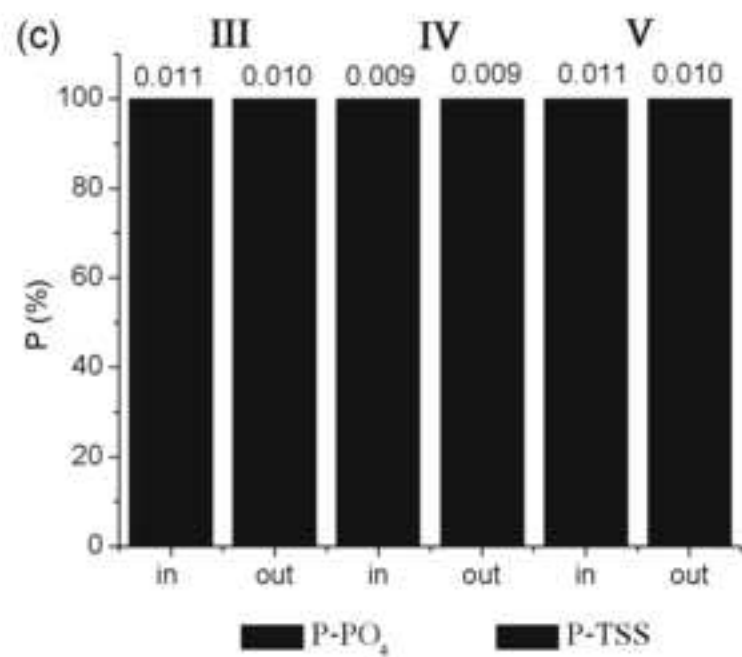
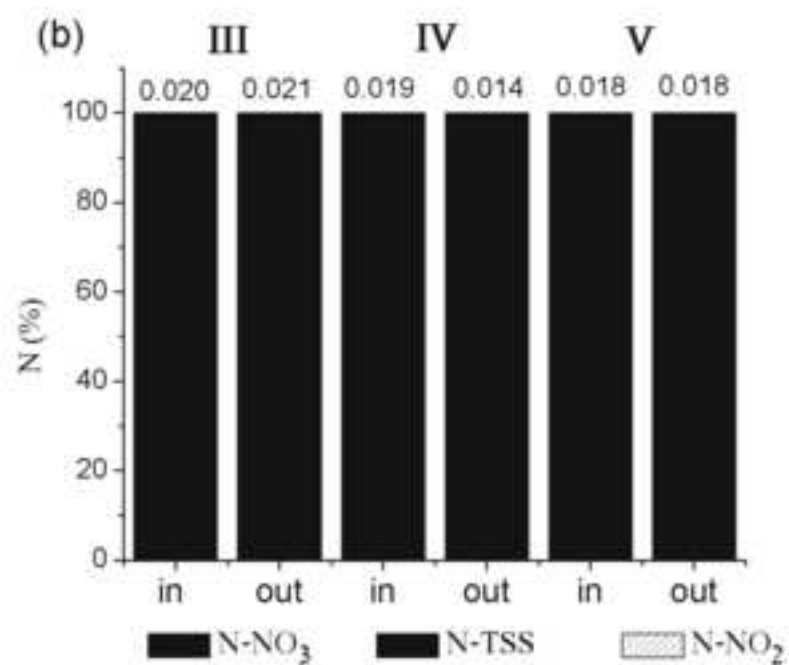
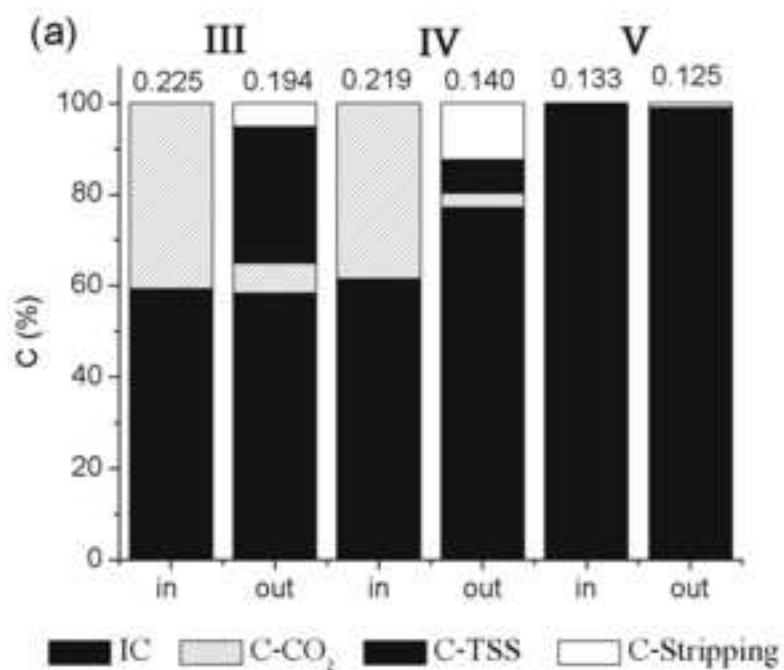


Figure 4
[Click here to download high resolution image](#)

